Metal Binding Modes of Alzheimer's Amyloid β-Peptide in Insoluble Aggregates and Soluble Complexes[†]

Takashi Miura, Kiyoko Suzuki, Naohito Kohata, and Hideo Takeuchi*

Graduate School of Pharmaceutical Sciences, Tohoku University, Aobayama, Sendai 980-8578, Japan

Received February 2, 2000

ABSTRACT: Aggregation of the amyloid β-peptide (Aβ) into insoluble fibrils is a key pathological event in Alzheimer's disease. Zn(II) induces the Aβ aggregation at acidic-to-neutral pH, while Cu(II) is an effective inducer only at mildly acidic pH. We have examined Zn(II) and Cu(II) binding modes of Aβ and their pH dependence by Raman spectroscopy. The Raman spectra clearly demonstrate that three histidine residues in the N-terminal hydrophilic region provide primary metal binding sites and the solubility of the metal−Aβ complex is correlated with the metal binding mode. Zn(II) binds to the N_τ atom of the histidine imidazole ring and the peptide aggregates through intermolecular His(N_τ)−Zn(II)−His(N_τ) bridges. The N_τ−metal ligation also occurs in Cu(II)-induced Aβ aggregation at mildly acidic pH. At neutral pH, however, Cu(II) binds to N_π, the other nitrogen of the histidine imidazole ring, and to deprotonated amide nitrogens of the peptide main chain. The chelation of Cu(II) by histidine and main-chain amide groups results in soluble Cu(II)−Aβ complexes. Under normal physiological conditions, Cu(II) is expected to protect Aβ against Zn(II)-induced aggregation by competing with Zn(II) for histidine residues of Aβ.

Amyloid β-peptide (Aβ)[1] is the major constituent of senile plaques in the brains of patients with Alzheimer's disease (AD) (*1*, *2*). The peptide is produced from a precursor membrane protein by normal proteolytic processing and is released into extracellular fluids as a soluble peptide of 39−42 amino acids (*3*−*5*). Under unknown conditions, Aβ aggregates and accumulates to form amyloid fibrils, whose extensive deposition causes neurodegeneration (*6*, *7*). Exposure to certain metal ions has been proposed as a risk factor for developing AD. The concentrations of Fe and Zn in multiple brain regions vulnerable in AD are elevated in AD patients compared to their age-matched controls (*8*−*10*), whereas the Cu concentrations are decreased (*8*). A recent microparticle-induced X-ray emission analysis has shown that Fe, Zn, and Cu are significantly concentrated in the neurophil of AD patients and are further concentrated within the core and periphery of senile plaques (*11*). Imbalances of metal ions may be related to the pathogenesis of AD.

Effects of metal ions on the aggregation of human Aβ have been studied in vitro. Al(III), Fe(III), and Zn(II) are known to promote aggregation of Aβ (*12*, *13*). Among them, Zn(II) induces significant Aβ aggregation at nearly physiological concentrations of the metal ion (*14*−*16*), implying participation of Zn(II) ions in the deposition of Aβ within amyloid plaques. Atwood et al. have recently demonstrated that Cu(II) is also a strong inducer of Aβ aggregation with a pH dependence different from that of Zn(II) (*17*). Zn(II) induces Aβ aggregation in a wide pH range (>6.0), whereas Cu(II) is effective only at pH 6.0−7.0.

Chemical modification and mutation studies have provided some information on the metal binding site of Aβ. The ability of both Zn(II) and Cu(II) to aggregate human Aβ is diminished by modifying all three histidine residues at positions 6, 13, and 14 with diethyl pyrocarbonate (*17*). Rat Aβ, which contains three amino acid substitutions, Arg5→Gly, Tyr10→Phe, and His13→Arg (*18*), binds Zn(II) and Cu(II) much less avidly than human Aβ (*15*, *17*). The reduced affinity of rat Aβ for Zn(II) is reproduced by the single His13→Arg mutation of human Aβ (*19*). Although these findings suggest that one or more of the histidine residues is involved in Aβ aggregation, little is known about the mode of metal binding.

In this study, we have examined the Zn(II) and Cu(II) binding modes of human Aβ in solution and in insoluble aggregates by Raman spectroscopy. Analysis of the Raman spectra has revealed two different modes of metal−Aβ binding. One is characterized by metal binding to the imidazole N_τ atom of histidine, which produces insoluble aggregates. The other involves metal binding to the N_π, but not N_τ, atom of histidine as well as to main-chain amide nitrogens, resulting in the formation of soluble complexes. Zn(II) binds to Aβ only in the former mode irrespective of pH. On the other hand, the Cu(II) binding mode is pH dependent. At mildly acidic pH, Cu(II) binds to Aβ in the former mode, whereas the latter mode is predominant at neutral pH. The transition from one binding mode to the other explains the strong pH dependence of Cu(II)-induced Aβ aggregation.

[†] This work was supported by Grant-in-Aid 09780593 from the Ministry of Education, Science, Sports, and Culture of Japan and by the Association for the Progress of New Chemistry (ASPRONC) Foundation.

* Corresponding author. Phone/Fax: +81-22-217-6855. E-mail: takeuchi@mail.cc.tohoku.ac.jp.

[1] Abbreviations: AD, Alzheimer's disease; Aβ, amyloid β-peptide; $A\beta_{1-40}$, 40-residue human Aβ; $A\beta_{1-16}$, N-terminal 16-residue fragment of $A\beta_{1-40}$; *R*, metal/peptide molar ratio.

10.1021/bi0002479 CCC: $19.00
Published on Web 05/19/2000

EXPERIMENTAL PROCEDURES

Materials. A 40-residue human Aβ peptide, Aβ_{1-40} (DAEFRHDSGYEVHHQKLVFFAEDVGSNKGAIIGLMVGGVV), and its N-terminal 16-amino acid fragment, Aβ_{1-16}, were synthesized on an automated peptide synthesizer (Applied Biosystems model 431A). The crude peptides were purified by HPLC on a reversed-phase column (Cosmosil 5C_{18}-AR). $ZnCl_2$ and $CuCl_2$ were purchased from Nacalai Tesque, Inc.

Preparation of Samples. The concentration of peptide was determined from the UV absorption intensity of tyrosine (ϵ_{275} = 1410 M^{-1} cm^{-1}) at pH 7.4. The metal complexes of Aβ_{1-40} and Aβ_{1-16} were prepared by adding 100 μL of aqueous $ZnCl_2$ or $CuCl_2$ (1.6 or 3.2 mM, pH ~4) to a 100 μL solution of the peptide (0.8 mM for Aβ_{1-40} and 3.2 mM for Aβ_{1-16}, pH 7.4) containing 16 mM NaCl. Then, the pH of the mixture solution was adjusted by adding a trace amount of 2 M aqueous NaOH or HCl. The metal−peptide mixture was incubated for 2 h at 22 °C and then centrifuged at 10000*g* for 1 h to sediment the aggregated particles. The precipitate was introduced into a glass capillary tube to record the Raman spectrum of the aggregates. Soluble complexes in the supernatant were concentrated for Raman measurements by lyophilizing a portion (50 μL) of the supernatant and then dissolving the lyophilized powder in 4 μL of deionized H_2O or D_2O (Isotec Inc.). The resulting solution contained 0−5.0 mM Aβ_{1-40} or 0−20.0 mM Aβ_{1-16} depending on the degree of aggregation. In D_2O, labile protons of the peptide were readily exchanged with deuterons both for the soluble complexes and for insoluble aggregates, as judged from the Raman spectra.

Aggregation Assays. The percentage of aggregated peptide was estimated from the amount of peptide remaining in the supernatant. The peptide in the supernatant was concentrated in the same way as described above except that 0.5 M aqueous HCl, instead of deionized H_2O, was used to dissolve the lyophilized powder. In the highly acidic solution, the metal ions were depleted from the peptide. The concentration of peptide was determined from the Raman intensity of the ~1445 cm^{-1} C−H bending band of CH_2 and CH_3 in the peptide relative to that of a band at 1640 cm^{-1} of the solvent water by using a predetermined standard curve of the Raman intensity versus peptide concentration.

Raman Spectroscopy. Raman spectra were excited with the 514.5 nm line of an Ar^+ laser (Coherent Innova 70) and recorded on a Jasco NR-1800 spectrometer equipped with a liquid nitrogen cooled CCD detector. Wavenumber calibration was effected by using the indene Raman spectrum, and the wavenumbers of sharp Raman bands were reproducible to within ±0.5 cm^{-1}. The intensities of Raman spectra were normalized by using the C−H bending band at ~1445 cm^{-1}. The solvent Raman bands were subtracted after the intensity normalization. Although the Raman spectra were recorded in the 1750−720 cm^{-1} interval, no appreciable effect of metal coordination was observed below 1200 cm^{-1}. Accordingly, the spectra in the 1750−1180 cm^{-1} interval only are presented here.

RESULTS

Zn(II) and Cu(II) Binding Modes of Aβ_{1-40}. The Raman spectrum of an aqueous solution of metal-free Aβ_{1-40} exhibits a very sharp amide I band at 1668 cm^{-1} and a strong amide III band at 1240 cm^{-1}, indicating that the peptide predominantly forms a β-strand (Figure 1A) (*20*−*22*). Although Raman scattering from the imidazole side chain of histidine is weak, a band at 1570 cm^{-1} can be assigned to the C_4═C_5 stretching vibration of the imidazole ring (*23*), which is known to exhibit a frequency upshift on metal binding (*24*, *25*). Phenylalanine Raman bands are also seen at 1604 and 1586 cm^{-1} (*21*).

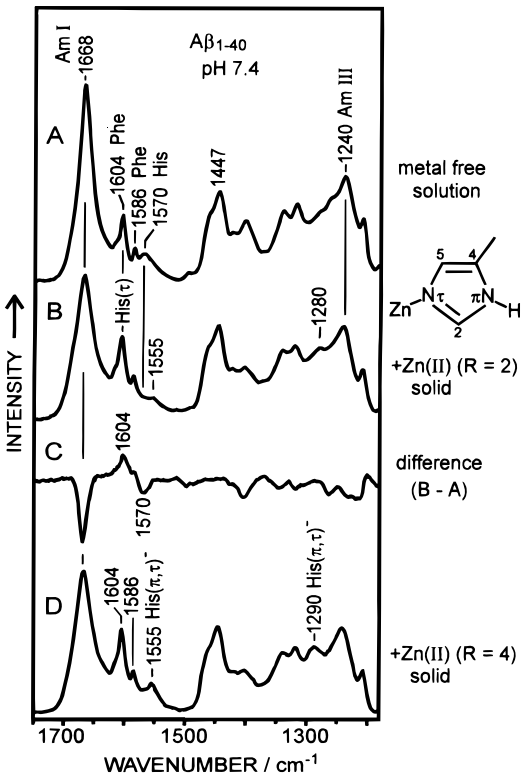

FIGURE 1: Raman spectra of metal-free Aβ_{1-40} and Zn(II)−Aβ_{1-40} aggregates. (A) Metal-free solution at pH 7.4. (B) Insoluble aggregates precipitated from a Zn(II)−Aβ_{1-40} mixture solution (pH 7.4) at R = 2. (C) The difference, B − A. (D) Insoluble aggregates precipitated from a Zn(II)−Aβ_{1-40} mixture solution (pH 7.4) at R = 4. The assignments of Raman bands are denoted as follows: His, metal-free histidine; His(τ), histidine bound to metal via N_τ; His(π,τ)$^-$, metal-bridging histidinate; Phe, phenylalanine; Am I, amide I; Am III, amide III. The Raman intensities of the spectra are normalized by using the 1447 cm^{-1} C−H bend band as an internal intensity reference. The structure of the His(τ) side chain is shown on the right side of the figure.

In agreement with the previous observation by Bush et al. (*14*, *15*), Zn(II) induced an extensive aggregation of Aβ_{1-40} at pH 7.4: about 80% and almost 100% of Aβ_{1-40} were precipitated by Zn(II) at metal/peptide molar ratios (R) of 2 and 4, respectively. Figure 1B shows the Raman spectrum of the insoluble Zn(II)−Aβ_{1-40} aggregate precipitated at R = 2. Upon binding of Zn(II), the amide I band becomes broader and weaker. Similar broadening is also seen for the amide III band. However, the peak positions of the amide bands are not affected by Zn(II) binding, suggesting that the peptide aggregates in β-sheet structure, which is the predominant structural component in amyloid fibrils of AD (*26*). The broadening of the amide bands may be ascribed to an inhomogeneous β-sheet formation and the weakening of the amide I band to an effect arising from stacking of β-sheets in the solid aggregate (*26*).

The effects of Zn(II) binding are also seen for histidine Raman bands. The 1570 cm^{-1} band of metal-free histidine is diminished in the spectrum of insoluble aggregates, and concomitantly a band at 1604 cm^{-1} gains intensity (Figure 1B). The intensity increase of the 1604 cm^{-1} band is likely to be caused by a shift of the histidine band from 1570 to 1604 cm^{-1}, where a phenylalanine band originally resides. This interpretation is confirmed by the appearance of a negative peak at 1570 cm^{-1} and a positive peak at 1604 cm^{-1} in the difference spectrum, ($R = 2$) − ($R = 0$) (Figure 1C). Recently, we have found that the wavenumber of the C_4═C_5 stretch vibration of histidine is sensitive to the site of metal binding: 1580 ± 10 cm^{-1} in the N_π−metal form and 1600 ± 6 cm^{-1} in the N_τ−metal form (*24*, *25*). The positive peak at 1604 cm^{-1} in the difference spectrum indicates that Zn(II) binds to the N_τ atom of histidine in the insoluble Zn(II)−Aβ_{1-40} aggregate. The binding of Zn(II) to the histidine N_τ atom may be a key step in peptide aggregation.

A weak band becomes detectable at 1555 cm^{-1} in the spectrum of the insoluble aggregate at $R = 2$ (Figure 1B). However, the difference spectrum ($R = 2$) − ($R = 0$) does not exhibit any peak around 1555 cm^{-1} (Figure 1C), suggesting that the same band is buried under the envelope of the histidine 1570 cm^{-1} band at $R = 0$ (Figure 1A). Possibly, the 1555 cm^{-1} band is ascribed to the antisymmetric stretching vibration of COO^- groups of the peptide C-terminus, three aspartates, and three glutamates (*21*). When the concentration of Zn(II) is elevated from $R = 2$ to 4, the intensity at 1555 cm^{-1} increases (Figure 1D), suggesting that an additional band emerges at this wavenumber. A similar intensity increase is also seen at 1290 cm^{-1}. Both the 1555 and 1290 cm^{-1} bands are characteristic of the deprotonated form of histidine (histidinate) whose imidazolate ring bridges two metal ions through N_π- and N_τ-ligation (*27*). Deprotonation and additional metal binding at the N_π atom of histidine occur at high Zn(II) concentrations.

In contrast to the dramatic aggregation induced by binding of Zn(II), Cu(II) did not much reduce the solubility of Aβ_{1-40} at neutral pH. Only ∼5 and ∼60% of Aβ_{1-40} were precipitated by Cu(II) at $R = 2$ and 4, respectively. Figure 2 compares the Raman spectra of the insoluble aggregate and soluble complex of Cu(II)−Aβ_{1-40} prepared at $R = 4$, pH 7.4. The Raman spectrum of the aggregate (Figure 2A) is almost identical to that of the insoluble Zn(II)−Aβ_{1-40} aggregate at $R = 2$ (Figure 1B), indicating that metal binding to the N_τ atom of histidine is common to the insoluble aggregates. No imidazolate bridge is generated by Cu(II).

The Raman spectrum of the soluble Cu(II)−Aβ_{1-40} complex (Figure 2B) is different from that of the aggregate (Figure 2A). In the spectrum of the soluble complex, a new strong band appears at 1417 cm^{-1}. The intensity of the amide III band at 1240 cm^{-1} is also significantly decreased. These spectral features are consistently explained by deprotonation and metal-coordination of main-chain amide nitrogens. When amide nitrogen deprotonates, the amide I mode (C═O stretch) is replaced by the in-phase and out-of-phase stretching vibrations of C═O/C−N^- (*28*). The 1417 cm^{-1} band of the soluble Cu(II)−Aβ_{1-40} complex is assignable to the in-phase stretch, whereas the out-of-phase stretch (∼1610 cm^{-1}) is too weak to be detected in the Raman spectrum. Since the amide III mode mainly involves NH bending (*20*−*22*), it is reasonable to assume that deprotonation reduces the amide III band intensity. The amide I band is also expected to decrease in intensity upon amide deprotonation, but the intensity rather increases compared to that in the insoluble aggregate. This is probably because the intensity decrease associated with the deprotonation is covered by an intensity increase on going from the aggregated state in the solid to the isolated state in solution.

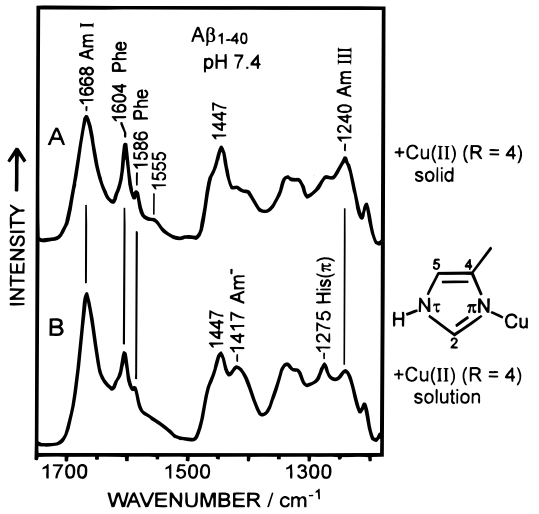

FIGURE 2: Raman spectra of insoluble aggregates and the soluble complex of Cu(II)−Aβ_{1-40}. (A) Insoluble aggregates precipitated from a Cu(II)−Aβ_{1-40} mixture solution (pH 7.4) at $R = 4$. (B) Soluble Cu(II)−Aβ_{1-40} complex in the supernatant of the same mixture solution. The assignments of Raman bands are denoted as follows: His(π), histidine bound to metal via N_π; Am^-, deprotonated amide bound to metal. For the others, see the caption to Figure 1. The Raman intensities of the spectra are normalized by using the 1447 cm^{-1} C−H bend band as an internal intensity reference. The structure of the His(π) side chain is shown on the right side of the figure.

The C_4═C_5 stretching band of the metal-free histidine at 1570 cm^{-1} is diminished in the Raman spectrum of the soluble Cu(II)−Aβ_{1-40} complex (Figure 2B) as in the case of the insoluble aggregate (Figure 2A), indicating that all three histidine residues are bound by Cu(II). Although the corresponding band of Cu(II)-bound histidine is not clearly seen owing to the overlap of phenylalanine bands at 1604 and 1586 cm^{-1}, the spectrum shows a distinct band at 1275 cm^{-1}, which is assignable to the ring-breathing mode of histidine. The ring-breathing mode of histidine is known to gain intensity when a metal ion binds to the N_π atom but not to the N_τ atom (*24*). The metal coordination of the N_π atom of histidine together with nitrogen atoms of deprotonated amides may be characteristic of the soluble Cu(II)−Aβ_{1-40} complex.

pH Dependence of Metal-Induced Aggregation of Aβ_{1-16}. Aβ_{1-40} consists of the N-terminal hydrophilic and C-terminal hydrophobic segments that can be cleaved between Lys16 and Leu17 by secretase (*3*). It is known that Aβ_{1-40} significantly aggregates near its isoelectric point (p$I = 5.3$) even in the absence of metal ions (*17*, *29*−*31*), possibly due to hydrophobic interactions among the C-terminal segments of peptides. The N-terminal hydrophilic segment itself is expected to be soluble in water. Accordingly, if the N-terminal peptide fragment, Aβ_{1-16}, aggregates in the presence of metal ions, the aggregation is attributable solely to metal−peptide interactions. We have examined the aggregation of Aβ_{1-16} in the absence and presence of Zn(II) and Cu(II) (R

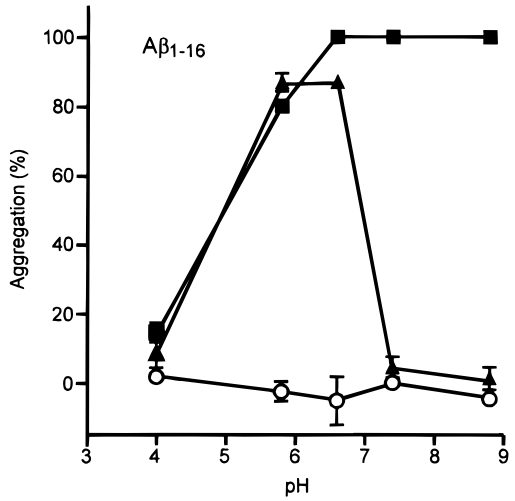

FIGURE 3: Effect of pH on Zn(II)- and Cu(II)-induced Aβ_{1-16} aggregation. Proportion of aggregated Aβ_{1-16} following incubation (22 °C, 2 h) at pH 4.0−8.8 with no metal (○), Zn(II) (6.4 mM, ■), and Cu(II) (6.4 mM, ▲). The starting peptide concentration was 1.6 mM. Data points are means ± SD, $n = 3$.

$= 4$). Figure 3 shows the results of aggregation assays. In the absence of metal ions, no aggregation of Aβ_{1-16} occurs over a wide pH range of 4.0−8.8. In the presence of Zn(II), however, Aβ_{1-16} is totally precipitated at pH 6.6−8.8. The proportion of aggregated Aβ_{1-16} still remains about 80% at pH 5.8, and a further acidification to pH 4 is required to recover the solubility of Aβ_{1-16}. On the other hand, Cu(II) induces aggregation of Aβ_{1-16} only at pH 6.6 and 5.8, and the peptide is highly soluble at pH 7.4, 8.8, and 4.0 (Figure 3). The pH dependence of Zn(II)- and Cu(II)-induced Aβ_{1-16} aggregation found here is in parallel with that reported for Aβ_{1-40} at millimolar concentrations except that aggregation due to C-terminal hydrophobic interactions around pH 5.3 is not seen for Aβ_{1-16} (*17*). Thus, Aβ_{1-16} is suitable for studying the role of metal ions in the aggregation of Aβ.

Another advantage of using Aβ_{1-16} is that histidine Raman bands are more clearly seen for Aβ_{1-16} than for Aβ_{1-40}. As described above, the C_4═C_5 stretching band of metal-bound histidine in Aβ_{1-40} is overlapped by stronger 1604/1586 cm^{-1} bands arising from three phenylalanine residues at positions 4, 19, and 20. Aβ_{1-16} has only one phenylalanine (Phe4), but still contains all three histidine residues (His6, His13, and His14).

Zn(II) Binding Mode of Aβ_{1-16}. The Raman spectrum of an H_2O solution of metal-free Aβ_{1-16} at pH 7.4 is shown in Figure 4A. The C_4═C_5 stretch vibration of metal-free histidine is clearly seen at 1574 cm^{-1} in this spectrum. The Y8a band of the single tyrosine residue at position 10 (Tyr10) is also evident at 1615 cm^{-1} (*21*). Figure 4B−D shows the Raman spectra of the Zn(II)−Aβ_{1-16} aggregates precipitated at pH 7.4, 6.6, and 5.8. The 1574 cm^{-1} band of metal-free histidine is absent in these spectra, and, instead, the band at 1604 cm^{-1} exhibits a significant intensity increase. The disappearance of the 1574 cm^{-1} band indicates that every histidine residue of Aβ_{1-16} is bound to Zn(II), and the intensity increase at 1604 cm^{-1} gives evidence that the Zn(II) binding site is N_τ. In addition to the intensity increase of the 1604 cm^{-1} band, two new bands appear at 1555 and 1290 cm^{-1} in the Raman spectra of the aggregates precipitated at pH 7.4 and 6.6 (Figure 4B,C). These bands are characteristic of the metal-bridging imidazolate (*27*) and indicate that N_π/N_τ-ligated histidinate coexists in the aggregates. At pH 5.8, on the other hand, the Raman bands of

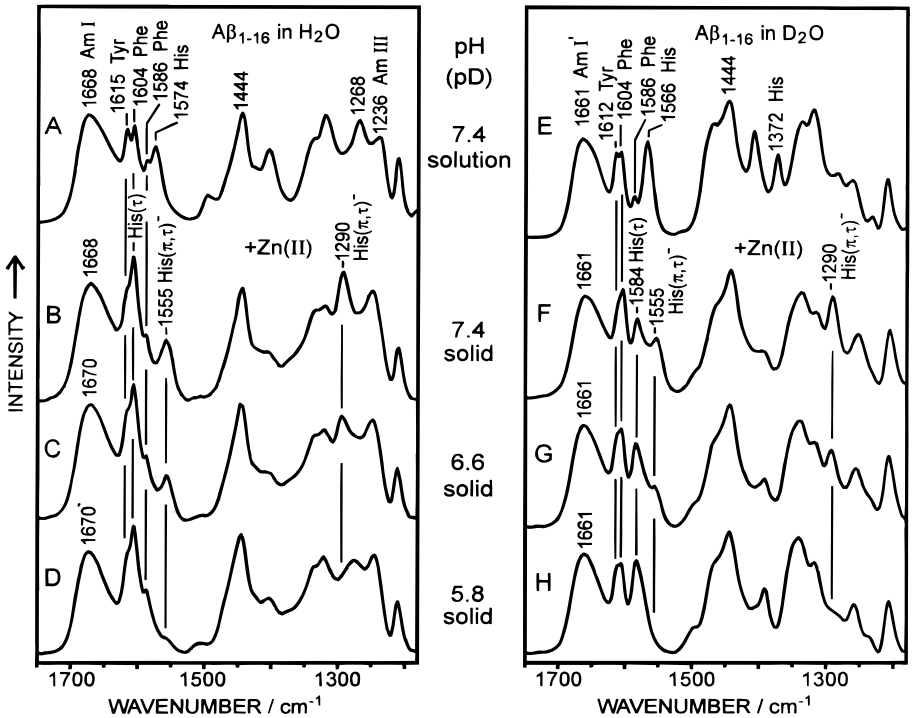

FIGURE 4: Raman spectra of metal-free Aβ_{1-16} and Zn(II)−Aβ_{1-16} aggregates. (A) Metal-free Aβ_{1-16} in H_2O solution (pH 7.4). (B) Zn(II)−Aβ_{1-16} aggregates precipitated from a mixture solution at $R = 4$, pH 7.4. (C) Aggregates precipitated at $R = 4$, pH 6.6. (D) Aggregates precipitated at $R = 4$, pH 5.8. (E−H) The same samples as A−D but prepared in D_2O. The assignments of Raman bands are denoted as in Figures 1 and 2. The Raman intensities of the spectra are normalized by using the 1444 cm^{-1} C−H bend band as an internal intensity reference.

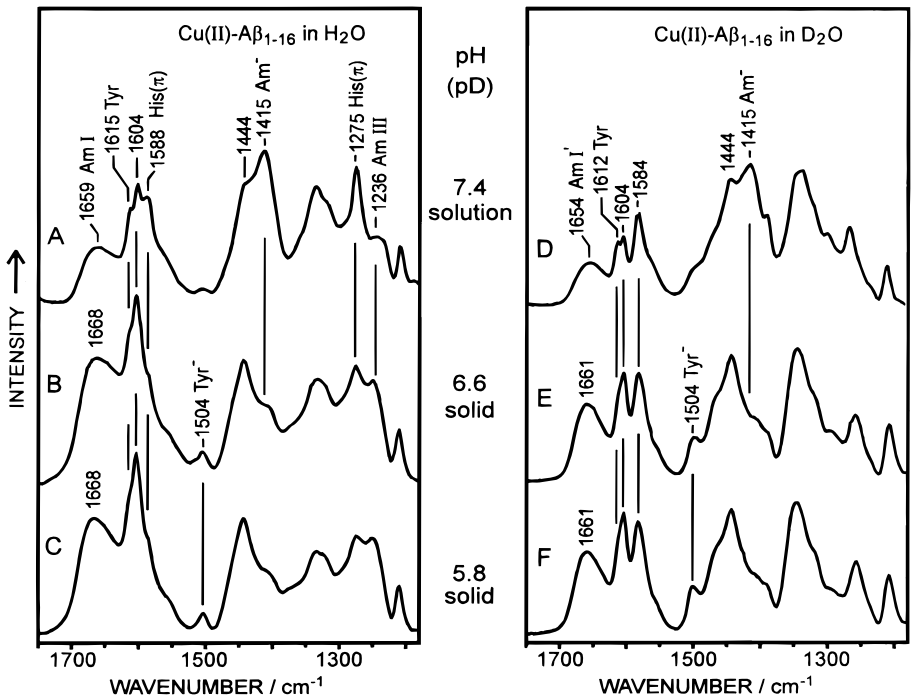

FIGURE 5: Raman spectra of the soluble complex and insoluble aggregates of Cu(II)−Aβ_{1-16}. (A) Cu(II)−Aβ_{1-16} in solution at $R = 4$, pH 7.4. (B) Cu(II)−Aβ_{1-16} aggregates precipitated from a mixture solution at $R = 4$, pH 6.6. (C) Aggregates precipitated at $R = 4$, pH 5.8. (D−F) The same samples as A−C but prepared in D_2O. The assignments of Raman bands are denoted as in Figures 1 and 2. The Raman intensities of the spectra are normalized by using the 1444 cm^{-1} C−H bend band as an internal intensity reference.

N_π/N_τ-ligated histidinate are almost diminished (Figure 4D), though the other Raman bands are not much affected by the acidification. Possibly, N_π/N_τ-ligated histidinate at pH 7.4 and 6.6 is converted to N_τ-ligated histidine at pH 5.8. The intensity increase at 1604 cm^{-1} expected from the conversion may be canceled out by a concomitant intensity decrease at the same wavenumber. Raman spectra in D_2O support this interpretation (vide infra).

The right panel of Figure 4 shows the Raman spectra of metal-free Aβ_{1-16} in D_2O solution and Zn(II)−Aβ_{1-16} aggregates precipitated from D_2O solutions (pD 7.4, 6.6, and 5.8) at $R = 4$. The C_4═C_5 stretch vibration of N-deuterated histidine is located at 1566 cm^{-1} (Figure 4E). Upon Zn(II) binding, this band disappears, and a new band appears at 1584 cm^{-1} (Figure 4F). Unlike N-hydrogenated histidine, the wavenumber of the C_4═C_5 stretch of N-deuterated histidine is not sensitive to the site of metal binding (*24*). However, the 1584 cm^{-1} band is assignable to N_τ-ligated, N_π-deuterated histidine because the Raman spectra of aggregates obtained from H_2O solution have shown that Zn(II) binds to the N_τ atom. The 1584 cm^{-1} band increases in intensity on going from pD 7.4 to 5.8 with a concomitant decrease of the 1555/1290 cm^{-1} bands of N_π/N_τ-ligated histidinate (Figure 4F−H). This observation confirms that Zn(II) is released from the N_π atom on going from pH 7.4 to 5.8, leaving N_τ-ligated histidine. Excess Zn(II) ions may bind to the N_π atoms of histidine residues at pH 7.4 and 6.6, whereas they do not bind to histidine at pH 5.8. Since 80% of Aβ_{1-16} is aggregated at pH 5.8 (Figure 3), the formation of N_π/N_τ-ligated histidinate may not be essential for Zn(II)-induced aggregation of Aβ. Actually, the histidinate Raman bands are absent in the Raman spectrum of the Zn(II)−Aβ_{1-40} aggregate precipitated at pH 7.4 and $R = 2$ (Figure 1B). They appear only for the aggregate precipitated at $R = 4$ (Figure 1D).

In D_2O, the Y8a band of tyrosine appears at 1612 cm^{-1} and shifts to 1604 cm^{-1} upon deprotonation (*21*). In the Raman spectrum of the Zn(II)−Aβ_{1-16} aggregate precipitated at pD 7.4 (Figure 4F), the intensity at 1612 cm^{-1} is decreased and that at 1604 cm^{-1} is increased compared to metal-free Aβ_{1-16} (Figure 4E), suggesting that Tyr10 is partially deprotonated and bound to Zn(II) in the aggregate. At pD 5.8 (Figure 4H), however, the 1612/1604 cm^{-1} intensity ratio is very close to that in the spectrum of metal-free Aβ_{1-16}, indicating that Zn(II) ions no longer interact with Tyr10 even in the aggregate. Tyr10 may not play an important role in Zn(II)-induced Aβ aggregation. In a previous paper (*15*), Tyr10 was proposed to be critical in Zn(II)−Aβ binding because iodination of Tyr10 decreased the susceptibility of Aβ to Zn(II)-induced aggregation. However, a recent mutational study has demonstrated that substitution of phenylalanine for Tyr10 does not affect the susceptibility of Aβ to Zn(II)-induced aggregation (*19*), which is consistent with the present Raman finding.

Cu(II) Binding Mode of Aβ_{1-16}. In contrast to Zn(II), Cu(II) induces Aβ_{1-16} aggregation in a strongly pH-dependent manner (Figure 3). Figure 5 shows the Raman spectra of the soluble complex at pH (pD) 7.4 and insoluble aggregates at pH (pD) 6.6 and 5.8. In all the spectra shown, the C_4═C_5 stretch band of metal-free histidine (1574 cm^{-1} in H_2O, Figure 4A; 1566 cm^{-1} in D_2O, Figure 4E) is absent, indicating that all histidine residues are bound to Cu(II). For the soluble complex at pH 7.4 (Figure 5A), strong bands are seen at 1588 and 1275 cm^{-1}, which are assignable to the C_4═C_5 stretch and ring-breathing modes, respectively, of Cu(II)−N_π-ligated histidine (*24*, *25*). Another strong band at 1415 cm^{-1} is ascribed to the in-phase stretch of C═O/C−N^- of deprotonated amide (*28*). These spectral features were also seen in the Raman spectrum of the soluble Cu(II)−Aβ_{1-40} complex at pH 7.4 (Figure 2B), though Raman

scattering from the hydrophobic C-terminal segment made the features less clear when the full-length peptide was used. It is concluded that Cu(II) binds to the N_π atom of histidine and to one or more deprotonated amide groups of the peptide main chain in the soluble Cu(II) complexes of both Aβ_{1-16} and Aβ_{1-40}.

The Raman spectra of the Cu(II)−Aβ_{1-16} aggregates precipitated from solutions at pH 6.6 (Figure 5B) and 5.8 (Figure 5C) are nearly identical to each other, but they are very different from that of the soluble complex at pH 7.4 (Figure 5A). The 1588 and 1275 cm^{-1} bands of N_π-ligated histidine are almost diminished in the spectra of the insoluble Cu(II)−Aβ_{1-16} aggregates. The C═O/C−N^- stretch band of deprotonated amide at 1415 cm^{-1} is also very weak. Instead, the band at 1604 cm^{-1} and the amide I band at 1668 cm^{-1} are greatly intensified. The spectra of the insoluble Cu(II)−Aβ_{1-16} aggregates bear strong resemblance with those of the Zn(II)−Aβ_{1-16} aggregates at the same pH values (Figure 4C,D), indicating that the major binding mode of Cu(II) to Aβ_{1-16} in the insoluble aggregates is analogous to that of Zn(II) to Aβ_{1-16}. In other words, Cu(II) binds mainly to the N_τ atom of histidine when insoluble aggregates are formed.

A notable difference between the Raman spectra of Zn(II)- and Cu(II)-induced aggregates of Aβ_{1-16} is that the 1604 cm^{-1} band is stronger when the aggregation is induced by Cu(II). It is also noted that a new band appears at 1504 cm^{-1} in the Raman spectra of Cu(II)−Aβ_{1-16} aggregates (Figure 5B,C). Analogous differences are also seen between the corresponding Raman spectra of aggregates precipitated from D_2O solutions (compare Figure 5E,F with Figure 4G,H). These differences can be explained by assuming the presence of tyrosinate in the insoluble Cu(II)−Aβ_{1-16} aggregates. The Y8a and Y19a bands of tyrosinate are expected at about 1604 and 1525 cm^{-1}, the former being strong and the latter very weak in visible-light-excited Raman spectra (*21*). When the deprotonated phenolic oxygen of tyrosinate is bound to a transition metal ion such as Cu(II) and Fe(III), the Y19a band shifts to about 1500 cm^{-1} and gains intensity through resonance with a π (phenolate) → *d* (metal) charge-transfer transition in the visible (*32*). [Such charge transfer does not occur for Zn(II), the *d* orbitals of which are fully occupied.] Accordingly, the 1504 cm^{-1} band in the Raman spectra of insoluble Cu(II)−Aβ_{1-16} aggregates (Figure 5B,C,E,F) is assigned to Cu(II)-bound tyrosinate, and the high intensity of the 1604 cm^{-1} band is ascribed to a contribution of the Y8a band of tyrosinate. Unlike Zn(II), Cu(II) binds to tyrosine in the insoluble aggregates of Aβ_{1-16}. Atwood et al. have shown that chemical modification of histidine in Aβ_{1-40} abolishes Zn(II)-induced aggregation completely but Cu(II)-induced aggregation only partly (*17*). Tyr10, located between His6 and His13, is likely to serve as a secondary metal binding site when Cu(II) induces Aβ aggregation.

Secondary Structure of Metal-Bound Aβ. Since both the aggregates of Zn(II)− and Cu(II)−Aβ_{1-16} give the amide I band at ∼1668 cm^{-1} (Figures 4 and 5), the peptide secondary structure in the insoluble aggregates is β-sheet as in the case of Aβ_{1-40}. On the other hand, the soluble Cu(II)−Aβ_{1-16} complex at pH 7.4 gives a broad band at ∼1660 cm^{-1} (Figure 5A), indicating a partial destruction of the β-sheet structure. In the Raman spectrum of the soluble Cu(II)−Aβ_{1-40} complex, a significant tailing to the low wavenumber side is seen for the amide I band peaking at 1668 cm^{-1} (Figure 2B). The Cu(II) binding to deprotonated amide may destroy the regular β-sheet structure in part of the N-terminal hydrophilic segment of Aβ_{1-40} but not affect the β-sheet structure of the C-terminal hydrophobic segment. The partial destruction of the β-sheet structure may be related to the increased solubility of Cu(II)−Aβ complexes at neutral pH.

DISCUSSION

The metal binding sites of Aβ revealed in this study are summarized in Figure 6A. All three histidine residues of Aβ are involved in the interaction with metal ions, and the metal−His(N_τ) ligation is a common feature among the insoluble Zn(II)− and Cu(II)−Aβ aggregates at pH 5.8−7.4 and 5.8−6.6, respectively. Both Zn(II) and Cu(II) are released from the N_τ atom by lowering the pH to 4.0 (data not shown), and the breakage of the metal−His(N_τ) bond leads to the recovery of the peptide solubility (Figure 3). These findings strongly suggest that the metal-induced aggregation of Aβ is promoted by cross-linking of the peptides through metal−His(N_τ) bonds, most likely through His(N_τ)−metal−His(N_τ) bridges at three histidine residues (Figure 6B). In the case of Cu(II)-induced Aβ aggregation, the single tyrosine residue is also involved as suggested by Raman spectroscopy. The tyrosine residue may assist the aggregation by forming Tyr(O^-)−Cu(II)−His(N_τ) bridges.

In the soluble complex formed between Cu(II) and Aβ at pH 7.4, histidine residues again act as ligands. In this case, however, the N_π atom, but not the N_τ atom, of histidine is bound by Cu(II). Additionally, deprotonated amide nitrogens of the main chain are also bound by Cu(II). Cu(II) is known to promote ionization of amide groups in peptides if a histidine residue is available as a primary binding site (*33*, *34*). A histidine residue and two or three deprotonated amides in the neighborhood can chelate a Cu(II) ion in a tetragonal geometry with Cu(II) being bound to the N_π atom of histidine (*34*). A similar chelation, depicted in Figure 6C, is likely to occur in the soluble Cu(II)−Aβ complex, and the distortion of peptide β-structure caused by the chelation may disfavor self-association of the peptide.

Aggregation assays in this study have shown that Zn(II) is a strong inducer of Aβ_{1-16} aggregation over a pH range from mildly acidic to basic, whereas Cu(II) is effective only at pH 5.8−6.6. This finding is in accord with that reported previously for Aβ_{1-40} (*17*). To explain the different pH effects on Cu(II)- and Zn(II)-induced aggregation, Atwood et al. hypothesized two classes of metal binding sites, one exposed for Zn(II) and the other buried for Cu(II). This hypothesis is not consistent with the present finding that all three histidine residues, the primary metal ligands, are bound by Cu(II) even in the soluble complex. The difference in pH dependence between Cu(II) and Zn(II) may be explained as follows. Due to an intrinsic propensity of Cu(II) to bind to main-chain amide nitrogens, intramolecular His(N_π)/amide(N^-)−Cu(II) chelation occurs around histidine residues of Aβ at neutral pH, and the chelation prevents the formation of intermolecularly cross-linked aggregates. Under mildly acidic conditions, however, the Cu(II)−amide(N^-) bond dissociates, and the Cu(II) ion is displaced from N_π to N_τ, which leads to aggregation of Aβ through His(N_τ)−Cu(II)−His(N_τ) bridges. In contrast, the Zn(II)−amide(N^-) ligation does not occur, and the His(N_τ)−Zn(II)−His(N_τ) bridges between peptide chains are maintained in a wide pH range.

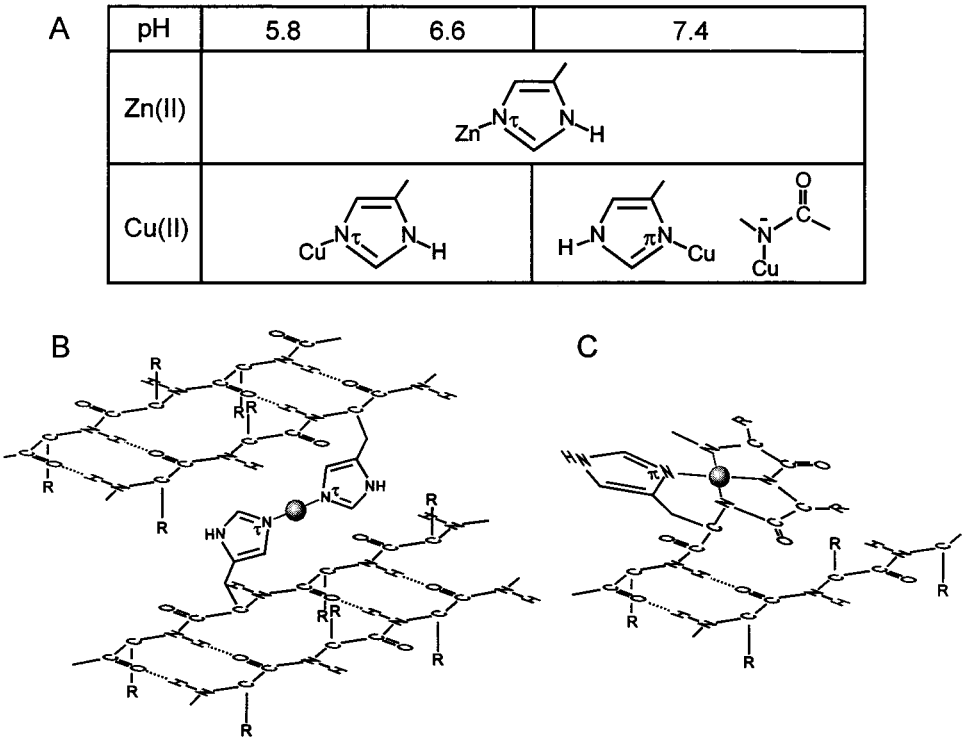

FIGURE 6: Metal binding mode of Aβ. (A) pH dependence of the Zn(II) and Cu(II) binding sites of Aβ. (B) A possible model for the insoluble aggregates of Zn(II)− and Cu(II)−Aβ formed at neutral-to-acidic and mildly acidic pH, respectively. β-Sheets of Aβ are cross-linked with His(N_τ)−metal−His(N_τ) bridges. (C) A model for the soluble Cu(II)−Aβ complex at neutral pH. The Cu(II) ion is coordinated by the N_π atom of a histidine residue and three deprotonated amide nitrogens. No cross-linking of β-sheets occurs. The metal ion is shown as a ball in panels B and C.

As shown by previous studies, Aβ preferentially and saturably binds Zn(II), and Zn(II) induces significant aggregation of Aβ even at its physiological concentrations in normal brain (*14*, *16*). Therefore, it may be reasonable to assume that the normal brain contains a factor that protects Aβ from Zn(II)-induced aggregation to avoid unwanted neurodegeneration. The Raman spectra of metal−Aβ complexes have demonstrated that the ability of a metal ion to induce Aβ aggregation correlates with the mode of metal−histidine binding. At neutral pH, Zn(II) prefers N_τ-ligation, while Cu(II) does N_π-ligation, both binding modes being competitive to each other. The ability of metal ions to displace the Zn(II) ion on Aβ has been examined at pH 7.4 (*35*). According to the displacement assay, Cu(II) is the most effective among the metal ions tested. Taken together, these results imply that Cu(II) may play a role in preventing Zn(II)-induced Aβ aggregation by maintaining Aβ in the soluble form with intramolecular His(N_π)/amide(N^-)−Cu(II) chelation. An appropriate balance of Zn(II) and Cu(II) concentrations in brain may be important to avoid Aβ aggregation. Unusual increase in Zn(II) concentration and decrease in Cu(II) concentration have been found in AD brains (*8*). In contrast to the preventive role of Cu(II) at neutral pH, Cu(II) induces aggregation of Aβ at mildly acidic pH as reported previously (*17*) and confirmed in this study. Under mildly acidic conditions, which might be produced by inflammatory mechanisms (*17*), Cu(II) can be a risk factor for AD by promoting Aβ aggregation together with Zn(II).

The Cu(II)−Aβ interaction is highly pH-sensitive, and analogous interactions have been found for other peptides. The octapeptide repeat, $(PHGGGWGQ)_n$, which occurs near the N-terminus of prion protein, has a high affinity for Cu(II) (*36*−*39*). Recently, we have found that the octapeptide is capable of forming a soluble complex with Cu(II) at neutral pH, in which the N_π atom of histidine together with deprotonated amide nitrogens act as ligands (*39*). Under mildly acidic conditions (pH ∼6), however, the Cu(II)−amide$^-$ linkage is broken, and the metal binding site of histidine switches from N_π to N_τ. Concomitant with the drastic change of the Cu(II) binding mode, the prion octapeptide repeat significantly aggregates. The pH dependence of the Cu(II)−prion interaction is strikingly similar to that of the Cu(II)−Aβ interaction found here. It may be possible that Cu(II) is commonly utilized for stabilizing the soluble form of a peptide that has a propensity to form pathogenic aggregates in brain.

REFERENCES

1. Masters, C. L., Simms, G., Weinman, N. A., Multhaup, G., McDonald, B. L., and Beyreuther, K. (1985) *Proc. Natl. Acad. Sci. U.S.A. 82*, 4245−4249.
2. Selkoe, D. J., Abraham, C. R., Podlisny, M. B., and Duffy, L. K. (1986) *J. Neurochem. 146*, 1820−1834.
3. Haass, C., Schlossmacher, M. G., Hung, A. Y., Vigo-Pelfrey, C., Mellon, A., Ostaszewski, B. L., Lieberburg, I., Koo, E. H., Schenk, D., and Teplow, D. B. (1992) *Nature 359*, 322−325.
4. Seubert, P., Vigo-Pelfrey, C., Esch, F., Lee, M., Dovey, H., Davis, D., Sinha, S., Schlossmacher, M., Whaley, J., and Swindlehurst, C. (1992) *Nature 359*, 325−327.
5. Shoji, M., Golde, T. E., Ghiso, J., Cheung, T. T., Estus, S., Shaffer, L. M., Cai, X. D., McKay, D. M., Tintner, R., and Frangione, B. (1992) *Science 258*, 126−129.
6. Pike, C. J., Burdick, D., Walencewicz, A. J., Glabe, C. G., and Cotman, C. W. (1993) *J. Neurosci. 13*, 1676−1687.
7. Lorenzo, A., and Yankner, B. A. (1994) *Proc. Natl. Acad. Sci. U.S.A. 91*, 12243−12247.

8. Deibel, M. A., Ehmann, W. D., and Markesbery, W. R. (1996) *J. Neurol. Sci. 143*, 137−142.
9. Danscher, G., Jensen, K. B., Frederickson, C. J., Kemp, K., Andreasen, A., Juhl, S., Stoltenberg, M., and Ravid, R. (1997) *J. Neurosci. Methods 76*, 53−59.
10. Cornett, C. R., Markesbery, W. R., and Ehmann, W. D. (1998) *Neurotoxicology 19*, 339−345.
11. Lovell, M. A., Robertson, J. D., Teesdale, W. J., Campbell, J. L., and Markesbery W. R. (1998) *J. Neurol. Sci. 158*, 47−52.
12. Kawahara, M., Muramoto, K., Kobayashi, K., Mori, H., and Kuroda, Y. (1994) *Biochem. Biophys. Res. Commun. 198*, 531−535.
13. Mantyh, P. W., Ghilardi, J. R., Rogers, S., DeMaster, E., Allen, C. J., Stimson, E. R., and Maggio, J. E. (1993) *J. Neurochem. 61*, 1171−1174.
14. Bush, A. I., Pettingell, W. H., Jr., Paradis, M. D., and Tanzi, R. E. (1994) *J. Biol. Chem. 269*, 12152−12158.
15. Bush, A. I., Pettingell, W. H., Multhaup, G., Paradis, M., Vonsattel, J. P., Gusella, J. F., Beyreuther, K., Masters, C. L., and Tanzi, R. E. (1994) *Science 265*, 1464−1467.
16. Esler, W. P., Stimson, E. R., Jennings, J. M., Ghilardi, J. R., Mantyh, P. W., and Maggio, J. E. (1996) *J. Neurochem. 66*, 723−732.
17. Atwood, C. S., Moir, R. D., Huang, X., Scarpa, R. C., Bacarra, N. M., Romano, D. M., Hartshorn, M. A., Tanzi, R. E., and Bush, A. I. (1998) *J. Biol. Chem. 273*, 12817−12826.
18. Johnstone, E. M., Chaney, M. O., Norris, F. H., Pascual, R., and Little, S. P. (1991) *Mol. Brain Res. 10*, 299−305.
19. Liu, S. T., Howlett, G., and Barrow, C. J. (1999) *Biochemistry 38*, 9373−9378.
20. Carey, P. R. (1982) *Biochemical Applications of Raman and Resonance Raman Spectroscopies*, Academic Press, New York.
21. Harada, I., and Takeuchi, H. (1986) in *Spectroscopy of Biological Systems* (Clark, R. J. H., and Hester, R. E., Eds.) pp 113−175, Wiley, Chichester, U.K.
22. Miura, T., and Thomas, G. J., Jr. (1995) *Subcell. Biochem. 24*, 55−99.
23. Ashikawa, I., and Itoh, K. (1979) *Biopolymers 18*, 1859−1876.
24. Miura, T., Satoh, T., Hori-i, A., and Takeuchi, H. (1998) *J. Raman Spectrosc. 29*, 41−47.
25. Miura, T., Satoh, T., and Takeuchi, H. (1998) *Biochim. Biophys. Acta 1384*, 171−179.
26. Kirschner, D. A., Abraham, C., and Selkoe, D. J. (1986) *Proc. Natl. Acad. Sci. U.S.A. 83*, 503−507.
27. Hashimoto, S., Ono, K., and Takeuchi, H. (1998) *J. Raman Spectrosc. 29*, 969−975.
28. Tasumi, M. (1979) in *Infrared and Raman Spectroscopy of Biological Molecules* (Theophanides, T. M., Ed.) pp 225−240, D. Reidel Publishing Co., Dordrecht, The Netherlands.
29. Burdick, D., Soreghan, B., Kwon, M., Kosmoski, J., Knauer, M., Henschen, A., Yates, J., Cotman, C., and Glabe, C. (1992) *J. Biol. Chem. 267*, 546−554.
30. Barrow, C. J., and Zagorski, M. G. (1991) *Science 253*, 179−182.
31. Fraser, P. E., Nguyen, J. T., Surewicz, W. K., and Kirschner, D. A. (1991) *Biophys. J. 60*, 1190−1201.
32. Tomimatsu, Y., Kint, S., and Scherer, J. R. (1976) *Biochemistry 15*, 4918−4928.
33. Bryce, G. F., Roeske, R. W., and Gurd, F. R. (1965) *J. Biol. Chem. 240*, 3837−3846.
34. Sundberg, R. J., and Martin, R. B. (1974) *Chem. Rev. 74*, 471−517.
35. Clements, A., Allsop, D., Walsh, D. M., and Williams, C. H. (1996) *J. Neurochem. 66*, 740−747.
36. Stöckel, J., Safar, J., Wallace, A. C., Cohen, F. E., and Prusiner, S. B. (1998) *Biochemistry 37*, 7185−7193.
37. Brown, D. R., Qin, K., Herms, J. W., Madlung, A., Manson, J., Strome, R., Fraser, P. E., Kruck, T., von Bohlen, A., Schulz-Schaeffer, W., Giese, A., Westaway, D., and Kretzschmar, H. (1997) *Nature 390*, 684−687.
38. Miura, T., Hori-i, A., and Takeuchi, H. (1996) *FEBS Lett. 396*, 248−252.
39. Miura, T., Hori-i, A., Mototani, H., and Takeuchi, H. (1999) *Biochemistry 38*, 11560−11569.

BI0002479